Nonlinear susceptibilities and polydispersivity in dipolar glasses

Joachim Hemberger, R. Böhmer, Alois Loidl

Angaben zur Veröffentlichung / Publication details:

Hemberger, Joachim, R. Böhmer, and Alois Loidl. 1998. "Nonlinear susceptibilities and polydispersivity in dipolar glasses." *Phase Transitions* 65 (1-4): 233–61. https://doi.org/10.1080/01411599808209289.

NONLINEAR SUSCEPTIBILITIES AND POLYDISPERSIVITY IN DIPOLAR GLASSES

J. HEMBERGER, R. BÖHMER* and A. LOIDL

Experimentalphysik V, Universität Augsburg, D-86135 Augsburg, Germany

The dipolar glass system D-$BP_{40}BPI_{60}$ was investigated using broadband dielectric spectroscopy over 12 decades in frequency and temperatures between $4\,K < T < 300\,K$. The complex dielectric constant reveals increasing polydispersivity with decreasing temperatures. However, no criticality can be detected in the linear components of the susceptibility: the distribution of relaxation times, as well as the mean relaxation time become infinite at $T=0$ only. The nonlinear susceptibility was followed over 4 decades of frequency. Again the mean relaxation times follow a pure Arrhenius-type behavior. However, from the extrapolation of the quasistatic nonlinear susceptibility a glass transition temperature of 30 K can be deduced in reasonable agreement with the Almeida–Thouless line determined from measurements of the FC/ZFC-susceptibilities. The frequency dependence of the real and imaginary parts of the third-order susceptibility cannot be described using simple extensions from Cole–Cole or Havriliak–Negami functions.

1 INTRODUCTION

Dipolar glasses (DG) (Höchli, 1987) are model systems to study the relaxation dynamics at the glass transition, which has remained one of the central problems in the physics of disordered systems. Supercooled liquids are disordered with respect to the center of mass lattice. Dipolar glasses reveal long-range translational order, but the electrical dipole

* Institut für Physikalische Chemie, Johannes-Gutenberg Universität, D-55099 Mainz, Germany.

moments, which randomly occupy the regular lattice sites, can freeze into a glassy state of random configurations below some freezing temperature T_f. Dipolar glasses can be regarded as the electrical analogue of magnetic spin-glasses (SG) and are a subspecies of orientational glasses (OG). OG are characterized by the freezing of multipolar moments, e.g. of quadrupolar or octupolar nature (Loidl and Böhmer, 1994). Dipolar glasses usually are realized in the form of mixed molecular crystals. Either a ferroelectric (FE) or antiferroelectric (AFE) compound is diluted by a material without dipolar moments, or one considers a mixed crystal of ferroelectric and antiferroelectric compounds. The latter possibility occurs in the system, which is presented in this work: a mixture of ferroelectric deuterated betaine phosphite (D-BPI) and antiferroelectric deuterated betaine phosphate (D-BP). The structural isomorphism of the pure betaine systems enables the growth of mixed crystals. These systems are addition compounds of the partially deuterated organic α-amino acid betaine and anorganic phosphorus groups phosphate $(CH_3)_3NCD_2COO{-}D_3PO_4$ or phosphite $(CH_3)_3NCH_2COO{-}D_3PO_3$ (Albers *et al.*, 1982; Albers, 1988; Fehst *et al.*, 1993). There exists a large family of betaine crystals with different adducts such as betaine calcium chloride dihydrogenphosphate (BCCD) or betaine arsenate (BA) showing different interesting order phenomena (Schaack, 1990). In D-BP : BPI the PO_3 and the PO_4 groups, respectively, are connected via hydrogen bonds and form quasi-one-dimensional zig-zag chains along the [010]-direction. The dipolar degrees of freedom are connected with the reorientational motion of the deuterons in the double-well potential of the hydrogen bonds. Actually there exist two inequivalent hydrogen bridges along and perpendicular to the [010]-direction. Because of this chain-like structure D-BP : BPI is a quite anisotropic (almost linear) dipole system, in contrast to the three-dimensional network of hydrogen bonds in the proton or deuteron glasses of the thoroughly studied KDP-type family, as e.g. rubidium ammonium dihydrogen phosphate (RADP) (Courtens, 1987).

The (x, T)-phase diagram of the D-BP : BPI system is shown in Fig. 1. In the case of low doping, long-range ordered structures are stabilized at both ends of the phase diagram, while higher defect concentrations lead to a glassy phase, where the dipoles are cooperatively frozen-in without long-range orientational order. The dipolar freezing

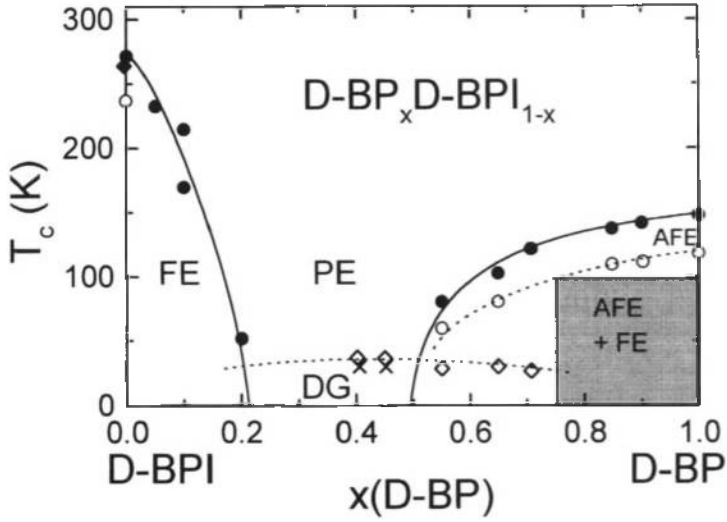

FIGURE 1 Phase diagram of deuterated betaine phosphate/betaine phosphite mixed crystals. The pure compounds reveal AFE and FE order, respectively. The shaded area corresponds to a regime with FE polarization characteristics. At intermediate concentrations an orientational glass state appears at low temperatures.

process is dominated by the interaction between the dipoles, "random bonds" (RB), and by spatially fluctuating static local fields of the environment, the so-called "random fields" (RF). Random fields often play an important role in dipolar glasses, which is a significant difference to magnetic spin glasses. The site disorder leads to the frustration of these interactions. Thus both, random fields and random bonds, have the tendency to suppress long-range orientational order. The relevant parameters to determine the properties of order behavior in such systems are the strength of the average dipolar interaction J_0 and the distribution width of the random bonds J as well as the random fields Δ. With growing influence of J and Δ the quenched system will tend to remain disordered in a glassy state. A central question concerning this freezing transition has to be answered: is it a static phenomenon or rather a kinetic effect which depends on the experimental time scale. To answer this problem, it is necessary to define an order parameter, which reflects the onset and the growth of glassy behavior. It is an advantage of dipolar model glasses, that in contrast to supercooled liquids such an order parameter can be defined via

the Edwards–Anderson order parameter $q = q_{EA} = \left[\langle \vec{p}_i \rangle^2\right]$ (Binder and Young, 1986), were $\langle \ldots \rangle$ denotes the time average for $t \to \infty$ and $[\ldots]$ the spatial average. Even if the macroscopic polarization $p = [\langle \vec{p}_i \rangle]$ is equal to zero, q will be finite if local dipolar degrees of freedom are frozen-in. For systems with symmetry breaking random fields the order parameter will be finite for all temperatures. A static glass transition will produce an additional contribution due to the cooperative freezing of the dipoles.

Unfortunately the order parameter cannot be determined directly in the experiment. Measurements of the linear dielectric response are a common method to investigate the dynamics of the freezing transition. The evaluation of the effective relaxation time τ often does not give any indication for a static freezing and reveals no critical behavior as it will be demonstrated for the D-BP : BPI system under consideration. But from this fact one cannot exclude the existence of a static transition, because the divergence τ would correspond to a freezing of the majority of the dipolar degrees of freedom. This condition does not have to be fulfilled necessarily. Glass transitions could be indicated by the fact that only the slow edge of the distribution of relaxation times diverges or the glass transition has to be described as a dynamic phase transition. Kutnjak *et al.* (1993) recently proposed an alternative way of analyzing the data from linear spectroscopy, yielding especially information about the behavior of the relaxation time-distribution at long times. In this work we deal especially with the behavior of the nonlinear susceptibility χ_{nl}, which is supposed to indicate an anomaly of the order parameter at the glass transition (Binder and Young, 1986) and reveals insight into the character of the dipolar glass transition. In what follows, we will describe in detail the temperature and frequency dependences of the nonlinear susceptibility.

2 THEORY AND MODEL CALCULATIONS

The field-dependent susceptibility can be defined as

$$\chi(E) \equiv P(E)/\varepsilon_0 E = \chi_1 + \chi_2 \cdot E + \chi_3 \cdot E^2 + \cdots. \tag{1}$$

The power expansion of $\chi(E)$ determines the nonlinear susceptibilities χ_N. In systems with inversion symmetry the even orders are

expected to vanish. For a harmonic input signal and for the case that the different susceptibility orders are separated with respect to the magnitude, one finds the real part χ'_N and the imaginary part χ''_N to be proportional to the corresponding Fourier components of the polarization signal. This offers a convenient way to evaluate the complex higher-order susceptibilities from the measured data. Since the imaginary parts of the nonlinear orders do not have the meaning of dissipative components, as is the case for the "loss" of the linear order, it may be a more vivid representation to show the data as magnitude $|\chi_N|$ and phase angle δ.

A different way to determine the nonlinear orders of the susceptibility is the use of a static bias field E_{Bias} modulated by a small ac field. Then the susceptibility at E_{Bias} is the local derivative of the polarization:

$$\chi_{E_{\text{Bias}}} \equiv \left.\frac{\partial P(E)}{\varepsilon_0 \partial E}\right|_{E_{\text{Bias}}} = \chi_1 + 2\chi_2 \cdot E_{\text{Bias}} + 3\chi_3 \cdot E_{\text{Bias}}^2 + \cdots . \quad (2)$$

Measuring $\chi_{E_{\text{Bias}}}$ for N different values of E_{Bias}, one can evaluate the first susceptibility orders χ_N. Both methods are only equivalent in the absence of hysteresis effects. Dispersion depends on the utilized method as well (Pirc *et al.*, 1994). Using the "bias"-method has the advantage that the contribution of the nonlinear susceptibility orders to $\chi_{E_{\text{Bias}}}$ at a static field E_{Bias} is higher than the contribution to $\chi(E)$ using a harmonic stimulation with the field amplitude $E_0 = E_{\text{Bias}}$. On the other hand we found that the sensitivity of the measurement with respect to the phase angles δ_N is higher, if large ac fields are utilized.

The significance of the nonlinear susceptibility in characterizing orientational glasses becomes clearer from a comparison with the linear susceptibility in ferroelectrics. In long-range ordered systems the FE transition is characterized by the critical temperature dependence of $\chi_1(T)$. The linear susceptibility is the derivative of the order parameter describing the ferroelectric transition, which is the polarization P. It measures the fluctuations of this order parameter. Within a mean-field (MF) or Landau-type approach it shows Curie–Weiss behavior:

$$\chi_1 \propto \frac{\partial P}{\partial E} \propto [\langle S_i S_j \rangle - \langle S_i \rangle \langle S_j \rangle] \underset{\text{MF}}{\propto} \frac{1}{|T - T_c|}. \quad (3)$$

In this case the corresponding third-order susceptibility scales with the 4th power of the linear, which again can be derived by a Landau expansion of the free energy of the system. So χ_{nl} reveals more pronounced anomalies at temperatures near the critical point than χ_l as illustrated in Fig. 2.

For a spin- or orientational-glass transition the Edwards–Anderson order parameter q_{EA} replaces the spontaneous polarization, which stays zero for all temperatures. The characteristic quantity in these systems is the spin-glass susceptibility (Chalupa, 1977):

$$\chi_{SG} = \frac{1}{T^2}\frac{\partial q_{EA}}{\partial [E^2]_z} \propto \left[(\langle S_i S_j\rangle - \langle S_i\rangle\langle S_j\rangle)^2\right]_z. \tag{4}$$

This is a derivative of the Edwards–Anderson order parameter and again measures the fluctuation order parameter. The experimental approach to this quantity is the nonlinear susceptibility. For the

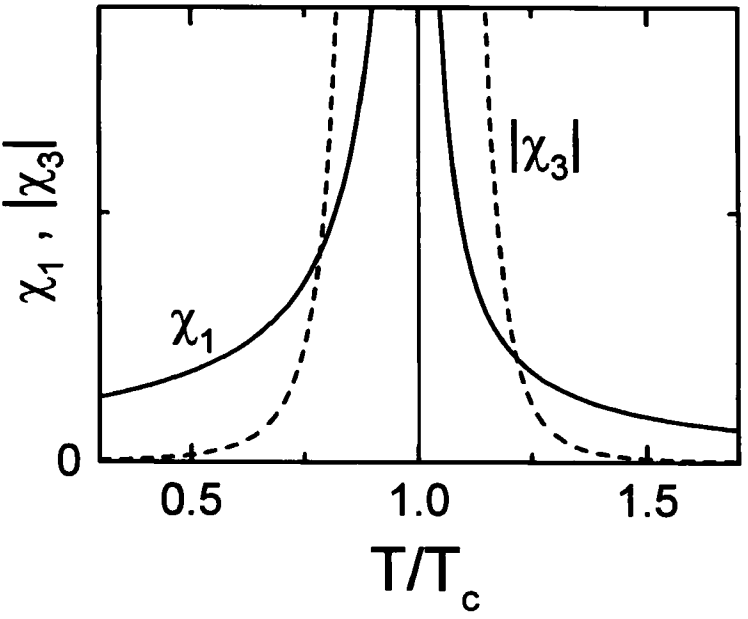

FIGURE 2 Linear (solid line) and nonlinear (dashed line) susceptibilities at a second-order ferroelectric transition according to the Landau theory.

average interaction strength $J_0 = 0$ it can be shown that (Binder and Young, 1986)

$$\chi_{\mathrm{nl}} \propto \frac{1}{T^3}\left(\chi_{\mathrm{SG}} - \frac{2}{3}\right). \tag{5}$$

The possible critical behavior of the spin-glass susceptibility should be directly reflected by the nonlinear susceptibility. For $J_0 \neq 0$, one can postulate the following temperature dependence within a phenomenological approach (Suzuki, 1977):

$$\chi_{\mathrm{nl}} \underset{\mathrm{MF}}{\propto} -\chi_1^4(T)\frac{1}{|T - T_{\mathrm{f}}|^{\gamma=1}}. \tag{6}$$

χ_{nl} measures not only the long-range correlations but in addition the critical behavior of the OG order parameter. This result is explicitly confirmed for random bond random field systems by the quasistatic limit of a dynamic MF-approach (Pirc *et al.*, 1994). These results are shown in Fig. 3. The freezing temperature T_{f} corresponds to the Almeida–Thouless line of stability, which separates the ergodic from the nonergodic regime, and determines a quasistatic freezing transition (de Almeida and Thouless, 1978). This temperature also can be determined by measurements of the "field cooled" (FC) and "zero-field cooled" (ZFC) susceptibility (Levstik *et al.*, 1991).

To estimate the frequency dependence of the nonlinear orders, one can use a phenomenological ansatz, which is an expansion of the linear response behavior of a Debye relaxator (Nakada, 1960). For a distribution of relaxation times this leads to the generalized Havriliak–Negami expression

$$\chi_N \propto (1 + (\mathrm{i}\omega\tau)^{\alpha})^{-N\beta}, \tag{7}$$

for the Nth order susceptibility (Orihara *et al.*, 1993). The results of this expression are illustrated in Fig. 4 in a Cole–Cole representation. The upper frame shows the behavior of a nonlinear Debye-relaxator for the first three orders. The well known half-circle for $N = 1$ spreads to the next quadrant for the orders $N > 1$ developing a spiral-like form. This is connected with a nonmonotonic shape of the real and

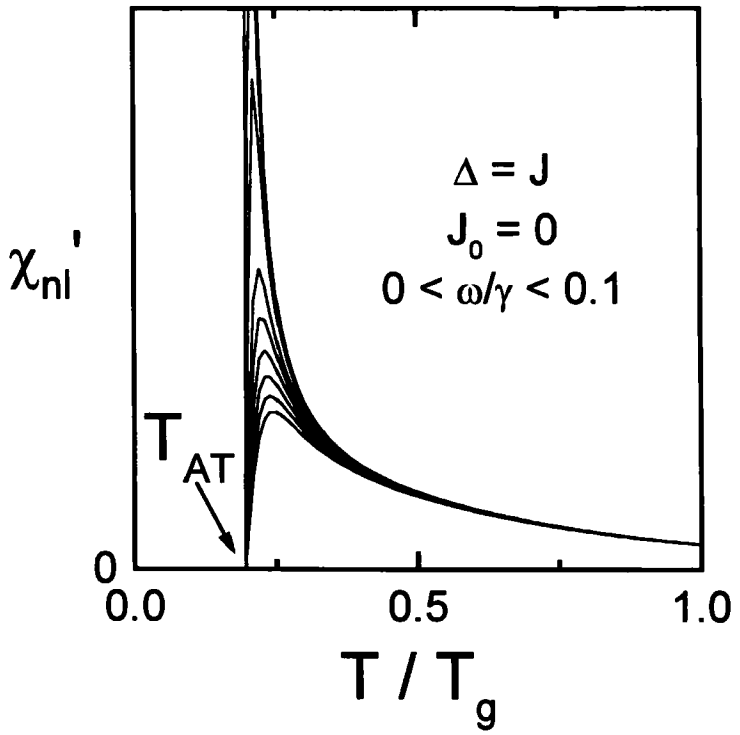

FIGURE 3 Real part of the nonlinear susceptibility according to a dynamic MF-Ansatz (Pirc *et al.*, 1994). Divergent behavior at the static freezing temperature is found for $\omega = 0$. The parameter γ is a generalized one-particle damping coefficient.

imaginary higher-order spectra and with the formation of additional extrema and roots. The positions of these significant points are listed in Table I.

It is important to note that the condition $\omega\tau = 1$ does not necessarily meet an extremum in the imaginary part of the higher orders, e.g. the condition $\chi_3' = 0$. The behavior of the third order of susceptibility is shown in the lower frame of Fig. 4 if polydispersivity is introduced. It can be seen that for broad and asymmetric distributions the extension of the Cole–Cole plots into the next quadrants is reduced.

The predictions of phenomenological response theory shown above are qualitatively similar to results from microscopic or thermodynamic models for liquid crystals and supercooled liquids (Alexiewicz, 1989; Déjardin *et al.*, 1993).

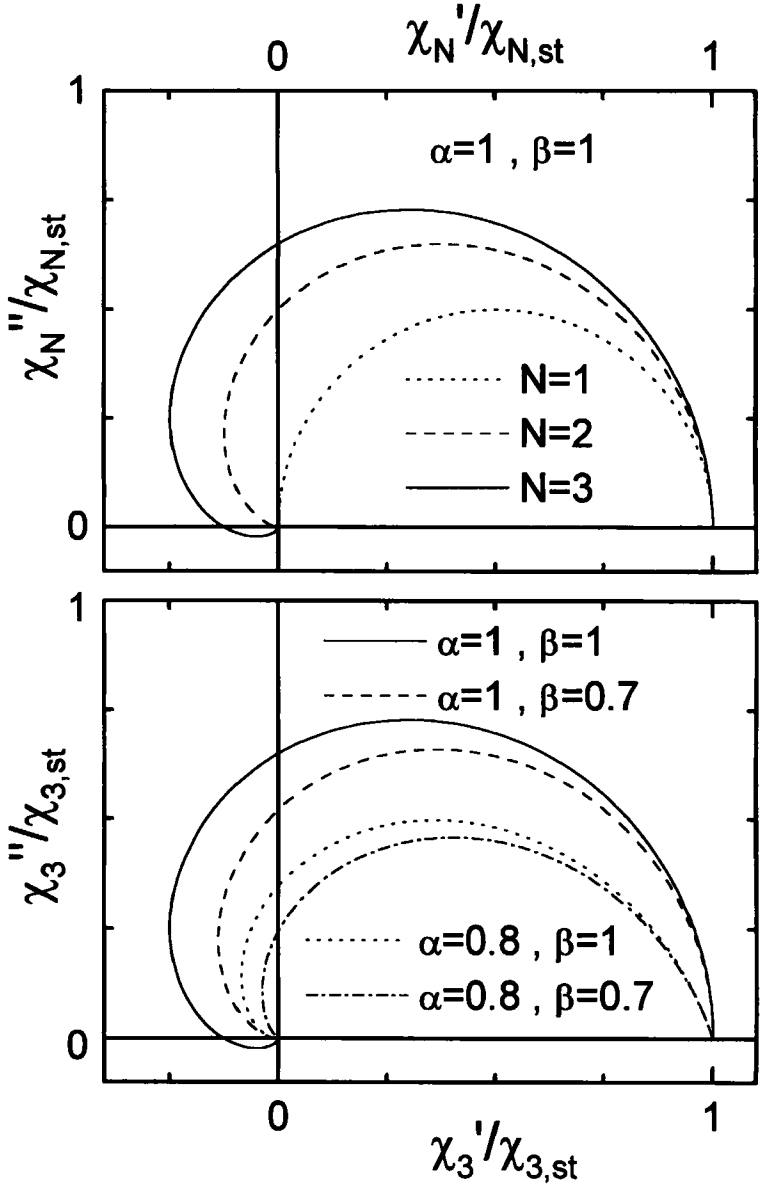

FIGURE 4 Cole–Cole representation of the normalized first, second and third susceptibilities of a Debye-relaxator according to relation 7 (upper frame). The lower frame shows the third order behavior for several values of the width parameter α and the asymmetry parameter β.

TABLE I Roots and extrema of the real and imaginary part of the linear and higher-order susceptibilities

Order	*Real part*	*Imaginary part*
Roots		
1	—	$\omega\tau = 0$
2	$\omega\tau = 1$	$\omega\tau = 0$
3	$\omega\tau = 1/\sqrt{3}$	$\omega\tau = 0, \sqrt{3}$
N	$\omega\tau = \tan[(2\pi k + \pi)/(2N)]$ with $k = 0, 1, 2, \ldots$ and $(2\pi k + \pi)/(2N) < \pi/2$	$\omega\tau = \tan(k\pi/N)$ with $k = 0, 1, 2, \ldots$ and $k\pi/N < \pi/2$
Extrema		
1	$\omega\tau = 0$	$\omega\tau = 1$
2	$\omega\tau = 0, \sqrt{3}$	$\omega\tau = 1/\sqrt{3}$
3	$\omega\tau = 0, 1$	$\omega\tau = \sqrt{2} - 1, \sqrt{2} + 1$
N	$\omega\tau = \tan[k\pi/(N+1)]$ with $k = 0, 1, 2, \ldots$ and $k\pi/(N+1) < \pi/2$	$\omega\tau = \tan[(2\pi k + \pi)/(2N+2)]$ with $k = 0, 1, 2, \ldots$ and $(2\pi k + \pi)/(2N+2) < \pi/2$

3 EXPERIMENTAL RESULTS

3.1 Crystal Growth and Sample Preparation

The single crystals were grown from an aqueous solution of betaine and H_3PO_3 and H_3PO_4, respectively, in a molar ratio of 1 : 1 by controlled evaporation at a constant temperature near 300 K. Deuteration was achieved by a three-cycle process of dilution with heavy water and subsequent distillation. The protons of all polar bonds (those of the phosphite complex and the carboxyl group of the betaine complex) can be substituted by deuterons. Thus the relevant protons of the crystal, that participate in the dipolar order–disorder phenomena, can be regarded as highly deuterated and a further deuteration of the organic complex should not affect the polar order behavior of the system (Brückner *et al.*, 1988). The crystals are colorless and transparent of optical quality and grow as (100)-plates with typical dimensions of about $5 \times 10 \times 20\,\text{mm}^3$. The samples were prepared as thin plates of a typical thickness $0.5\,\text{mm} \leq d \leq 1\,\text{mm}$ and a geometrical capacitance of $C_{\text{geo}} \approx 0.2\,\text{pF}$. The measurements presented in this work have been performed with an electric field E parallel to the [010] direction. The sample electrodes were prepared with silver paint on opposite sides of the samples.

3.2 Experimental Details

In the following we give some experimental details concerning the experimental setups used for the dielectric measurements presented in this work.

Most of the measurements were performed using a modified Sawyer–Tower circuit (Sawyer and Tower, 1929), in which the sample was connected in series with a reference capacitor whose capacitance C_r was at least by a factor of 1000 larger than that of the sample C_s (Hemberger, 1997). Across this circuit the driving signal is applied. Voltages from 1 V for linear measurements up to more than 1 kV for field-dependent measurements could be employed, depending on the geometry and quality of the sample. The voltage across the reference capacitor is a measure of the polarization P in the sample, while the voltage across the sample determines the macroscopic field E. An electrometer amplifier, with an input impedance $\geq 200\,\mathrm{T}\Omega$, was used as impedance transformer enabling the detection of $P(E)$ cycles in the mHz regime. In the case of a harmonic driving signal, the $P(E)$ data were recorded using a digital lock-in technique. A 14-bit multichannel AD-device allowed the phase sensitive determination of the driving field E and the polarization response P of the sample at frequencies in the mHz and Hz regime. The data were analyzed with standard Fourier-analysis algorithms (Dixon and Wu, 1989).

In the course of this work this kind of Sawyer–Tower circuit was used for three different experimental procedures:

(i) A symmetric, harmonically alternating electric field with a large amplitude E_0 was used for either detecting $P(E)$ hysteresis loops or evaluating this data in terms of linear and nonlinear harmonic components of the complex field-dependent dielectric susceptibility.

(ii) A small ac component superimposed on a dc bias field was utilized to determine $\varepsilon(T, E_{\mathrm{Bias}})$ via the analysis of the local derivative of $P(E_{\mathrm{Bias}})$.

(iii) In order to detect effects of thermo-remanent polarization cycles of zero-field cooling (ZFC), field heating (FH), field cooling (FC) and zero-field heating (ZFH) were applied. During each step the external field was held constant and the polarization was measured while ramping the sample temperature at a constant rate.

Rates of 1 and 2 K/min were used but no discernible differences could be detected.

Additional measurements of the complex linear dielectric constant ε^* were performed using the autobalance bridge HP4284A for frequencies $20\,\text{Hz} < \nu < 1\,\text{MHz}$ and the impedance analyzer HP4191A, which uses a coaxial line reflection technique for frequencies $1\,\text{MHz} < \nu < 1\,\text{GHz}$. Typical fields in these measurements were about 1 V/mm for $\nu < 1$ MHz and 0.05 V/mm for $\nu > 1$ MHz.

3.3 The Pure Deuterated Compounds: D-BP and D-BPI

Protonated betaine phosphate becomes antiferroelectric (AFE) below $T_{c2} = 87\,\text{K}$ and reveals a further structural phase transition of unknown origin at $T_{c3} = 83\,\text{K}$ (Albers *et al.*, 1982). The second phase transition produces a tiny anomaly in the linear dielectric susceptibility but can well be detected in heat capacity experiments (Fehst *et al.*, 1993). It has been speculated that at 83 K possibly the unit cell is doubled along the *a*-axis (Maeda *et al.*, 1989). Protonated betaine phosphite reveals a transition into a ferroelectric (FE) low-temperature phase at $T_{c2} = 200\,\text{K}$. The phase-transition temperature strongly depends on sample quality and differs by as much as 30 K. No further phase transition could be detected in the FE compound down to the lowest temperatures. Here we report on field-dependent measurements of the dipolar susceptibility especially focusing on the higher-order susceptibilities.

The polarization has been measured as a function of electric field for the deuterated betaine phosphate. The polarization loops were determined at a frequency of 18 Hz and fields of 666 V/mm. Representative results for three different temperature regions are shown in Fig. 5. Although D-BP orders antiferroelectrically a clear FE signature can be detected in the polarization at low temperatures. This FE component could be due to ordering processes of the second hydrogen bridge or due to the development of strong anisotropies in the dielectric properties. The resulting susceptibilities that have been deduced from these hysteresis loops are documented in Fig. 6 which shows the absolute value and the phase angle of the linear and third-order susceptibility of deuterated betaine phosphate. At high temperatures the linear susceptibility follows roughly a Curie–Weiss law

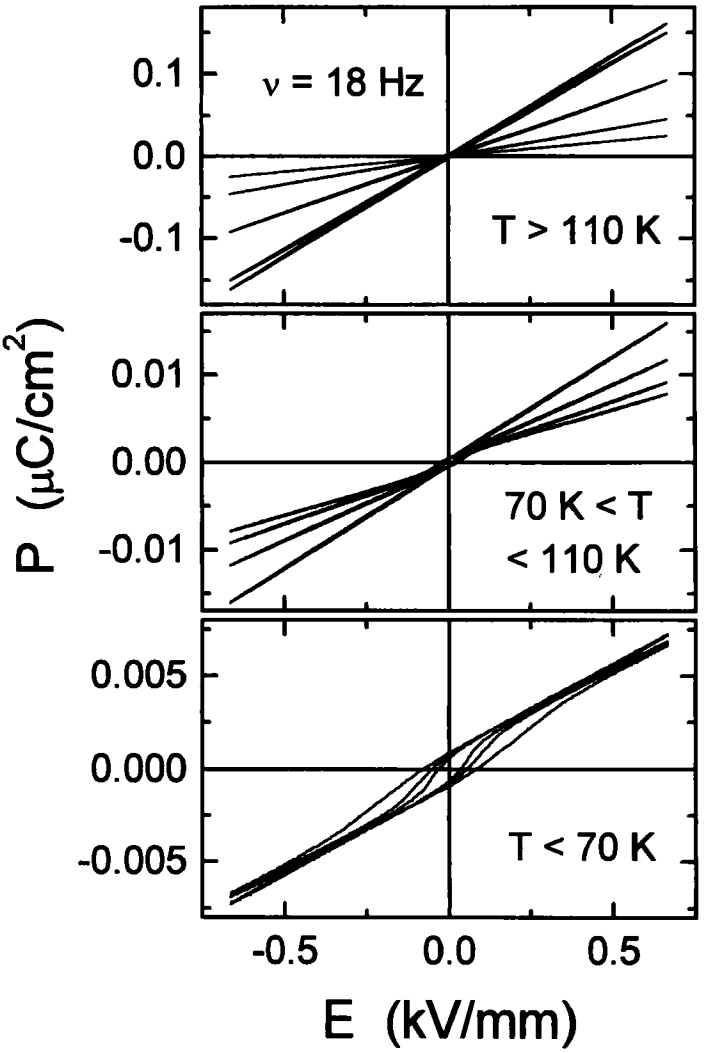

FIGURE 5 Polarization vs field in D-BP at three different temperature regimes.

with a characteristic Weiss temperature of 120 K. On cooling the paraelectric regime is followed by a cusp-shaped maximum close to 140 K and a strong decrease. The loss angle δ_1 is close to zero above 50 K and reveals an increase and a dispersion characteristic for relaxational or tunneling processes at low temperatures. These

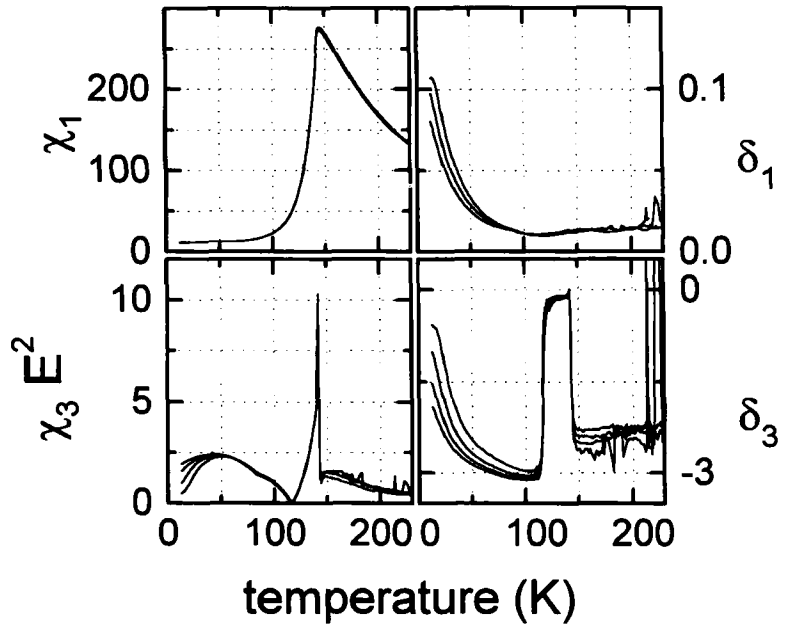

FIGURE 6 First and third-order of the susceptibility in D-BP. The measurements were performed using frequencies 113 mHz $< \nu <$ 134 Hz and a field amplitude $E_0 =$ 666 V/mm.

dispersion phenomena are unexpected in an antiferroelectrically ordered state. They may be due to the ordering of the second hydrogen bond that is perpendicular to the polar axis or due to defect states. The temperature dependences of the third-order susceptibility and phase angle reveal much more anomalies indicating a richer phase diagram than indicated in the linear susceptibility. The AFE phase transition at 145 K is indicated by sharp increase as well in the susceptibility as in the phase angle. A minimum in χ_3 and a sharp decrease in δ_3 signal a further phase transition. This phase transition seems to correspond to T_{c3} in the protonated compounds and again is of unknown origin. At low temperatures dispersion effects dominate also the third-order susceptibility.

To get further insight into effects connected with the stability of the ordered state in D-BPI, susceptibility measurements were performed using harmonic stimulation up to 167 V/mm, which is about the minimum value of E_c in the temperature range below 250 K. Results of

these measurements are reported in Fig. 7. The upper three pairs of frames show the linear order component of the dielectric susceptibility, χ_1, and the corresponding loss-angle, δ_1, for various field strengths and frequencies. A variety of features shows up in these data.

The peak related to the ferroelectric transition reveals a slight anomaly which increases with increasing field. Even a double peak structure develops for the loss angle at 56 V/mm at a probing frequency of 90 Hz and for χ_1 at high fields. The double peak

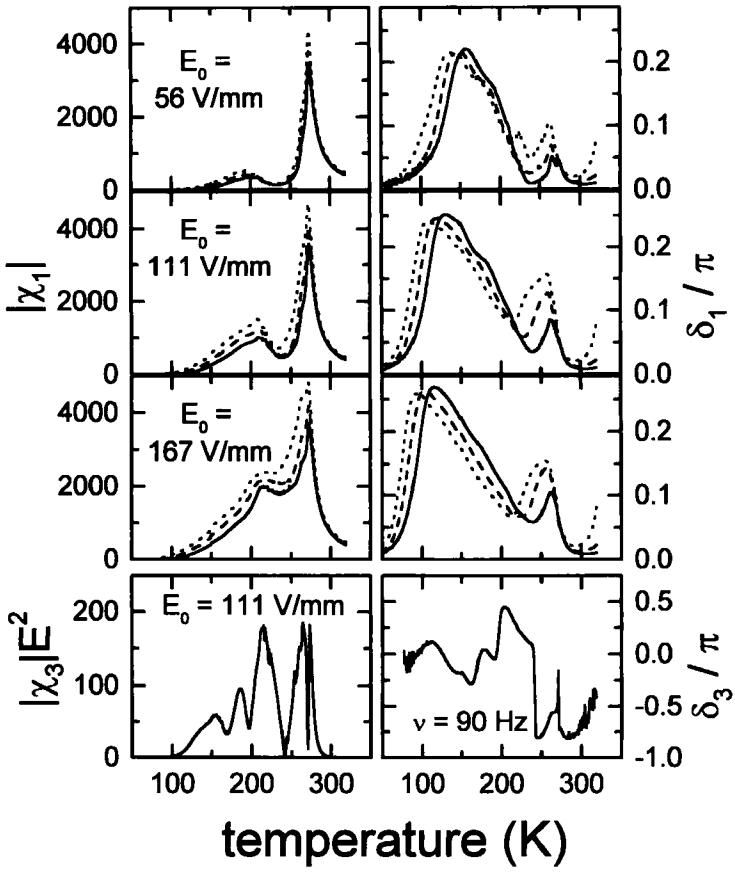

FIGURE 7 Three upper pairs of frames: Magnitude and loss angle of the first-order harmonic susceptibility of D-BPI for field amplitudes of 56 V/mm $< E_0 <$ 167 V/mm and frequencies $\nu = 0.77$ Hz (···), $\nu = 8.1$ Hz (- - -), $\nu = 90$ Hz (—). The lower pair shows a typical dataset of the corresponding third order terms.

structure probably signals the subsequent phase transitions at $T_{c2} = 272\,\mathrm{K}$ and $T_{c3} = 266\,\mathrm{K}$. Just below the ferroelectric phase transition dispersion effects develop which increase with frequency. This effect indicates domain-wall relaxation processes at these relatively high fields.

The sequence of phase transitions, T_{c2} and T_{c3}, near 270 K is well documented in the magnitude of the third-order susceptibility χ_3 (lower pair of frames) where a peak doublet shows up. Also the related peak in the corresponding phase angle δ_3 at 272 K seems to be accompanied by a satellite peak at 266 K.

The second feature of the data presented in Fig. 7 is the existence of an additional low-temperature dispersion in χ_1 ($100\,\mathrm{K} < T < 250\,\mathrm{K}$), which is accompanied by a peak in δ_1. The position of this peak appears to be frequency and field-dependent. It is reasonable, that for higher fields the relaxing entities stay mobile down to lower temperatures as is indeed observed in Fig. 7. The evaluation of the peaks in δ_1 leads to a field-dependent thermally activated process. The corresponding effective energy barrier E_B decreases from about 5300 K for low field-amplitudes to about 2300 K with an attempt frequency $\nu_0 \approx 2 \times 10^{11}\,\mathrm{Hz}$ for $E_0 = 167\,\mathrm{V/mm}$.

An additional characteristic feature in Fig. 7 is a sharp jump in the third-order loss angle δ_3 from a value near $-\pi$ (which indicates a ferroelectric curvature of the $P(E)$-curves with increasing field) to values near zero (which signals the growing steepness of the $P(E)$-curves with increasing field-magnitude in an antiferroelectric fashion) at $T \approx 250\,\mathrm{K}$. The observed behavior highly suggests the existence of a further phase transition at $T_{c4} = 250\,\mathrm{K}$. In addition there is a number of further features, which can be seen in Fig. 7: (i) $|\chi_1|$ shows a distinct maximum near 210 K, which is accompanied by a marked peak in $|\chi_3|E^2$. (ii) There is a multiple peak structure in the magnitude of the third-order susceptibility χ_3 and of the corresponding phase angle δ_3 below T_{c4}, which we found to be field-dependent. Up to now we have no explanation for these additional features but they may well reflect the complexity of the related domain dynamics or a complicated sequence of polar phase transitions.

Figures 6 and 7 provide clear experimental evidence that the higher-order susceptibilities give a precise signature of phase transitions which are hidden in first order.

3.4 The Dipole Glass D-$BP_{40}BPI_{60}$

As can be seen from the x, T-phase diagram (Fig. 1), at intermediate concentrations, the mixed compounds reveal no long-range polar order at low temperatures. In this concentration regime the dipoles freeze into random configurations. Here we present dielectric results for the deuterated compound D-BP40 : BP60 focusing especially on the nonlinear dispersion. As background information the real and imaginary parts of the dielectric constant are shown in Fig. 8 (Loidl *et al.*, 1996) where the dielectric constant and the dielectric loss are plotted as functions of frequency for different temperatures between 13 and 83 K. Figure 8 reveals the characteristic signature of the slowing down of a dipolar system. The dispersion steps and the loss peaks are almost symmetric but broaden considerably as the temperature is lowered. To gain a qualitative analysis the dispersion steps and the loss peaks were fitted simultaneously using the phenomenological Havriliak–Negami function which allows for a symmetric broadening (width parameter α) and for an asymmetry (asymmetry parameter β). The temperature dependencies of both parameters are shown in Fig. 9. The symmetry parameter extrapolates to zero at 0 K indicating an infinite width of the distribution of relaxation rates at zero temperature. The asymmetry parameter is almost temperature independent and close to unity indicative of a rather symmetrically broadened Cole–Cole type of relaxation. The linear increase of the width parameter can perfectly well be described assuming a temperature independent distribution of energy barriers, due to local random fields. Cooperativity or hierarchical relaxation may be hidden in the asymmetry parameter. It is interesting to note that the mean relaxation rate follows an Arrhenius type of behavior (see inset of Fig. 8). The Arrhenius law is characterized by an attempt frequency of $\nu_0 = 3.14$ THz and by an energy barrier $E_B/k_B = 822$ K. Thus, at first sight no criticality at all can be detected in the linear susceptibility. Phenomenologically finite freezing temperatures are often claimed if Vogel–Fulcher behavior is observed in the temperature dependence of the mean relaxation rate or if the width of the distribution of relaxation times diverges at finite temperatures. We have shown earlier (Hemberger *et al.*, 1996) that using a representation of Kutnjak *et al.* (1993) a finite glass transition temperature of 30 K follows from the data of the linear susceptibility.

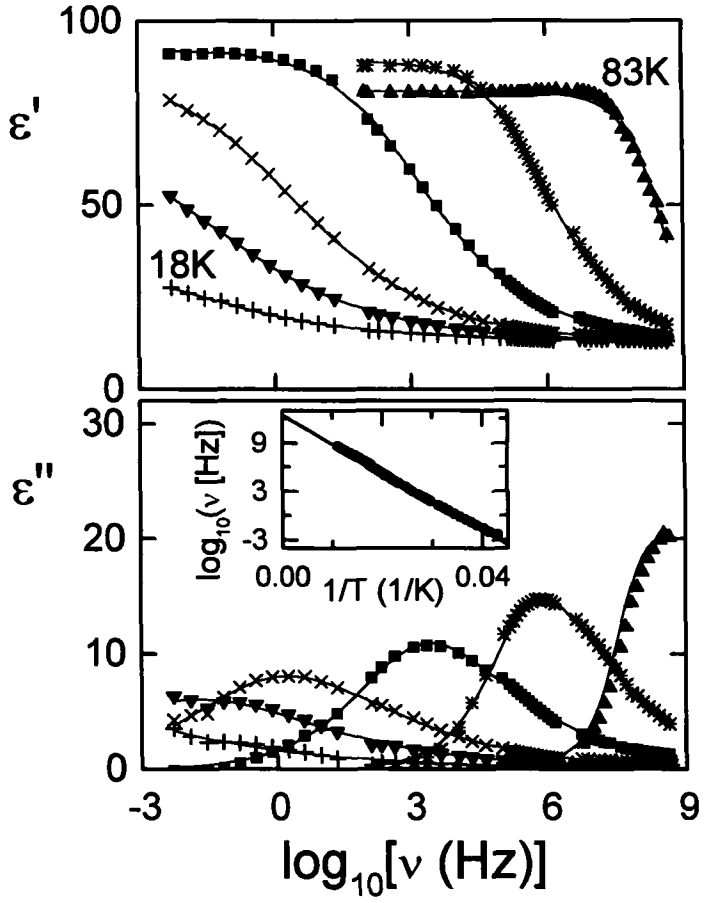

FIGURE 8 Frequency dependence of the real part (upper frame) and the imaginary part (lower frame) of the complex dielectric constant in D-$BP_{40}BPI_{60}$ measured for frequencies $5\,\text{mHz} < \nu < 200\,\text{Hz}$ and for temperatures $T = 18, 23, 28, 38, 53$ and 83 K. The lines are fits using the Havriliak–Negami distribution of relaxation times. The inset shows an Arrhenius representation of the loss-maxima. The effective activation-barrier is $E_B = 822\,\text{K}/k_B$ and the corresponding attempt frequency $\nu_0 = 3.14\,\text{THz}$.

In this communication we will focus on the temperature and frequency dependencies of the components of the nonlinear susceptibilities.

Before doing so we would like to determine the Almeida–Thouless (AT) line for this dipolar glass. In finite external fields the AT line separates the ergodic high-temperature phase from the nonergodic glassy phase at low temperatures. Generally the AT line can be

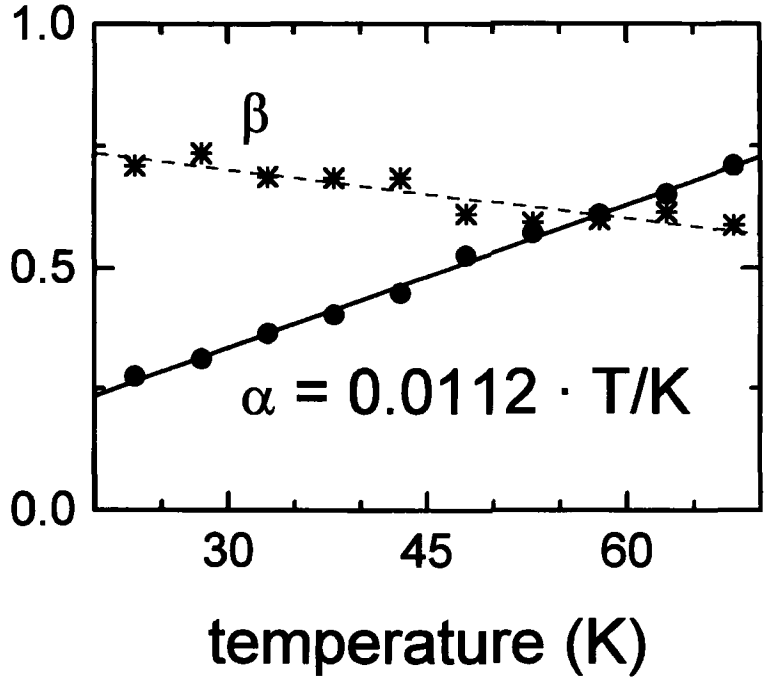

FIGURE 9 Temperature dependence of the width parameter α and the asymmetry parameter β of the Havriliak–Negami distribution.

determined through measurements of the field cooled and zero-field cooled susceptibilities under quasistatic conditions. The two quantities are expected to split at the AT line. A representative FC and ZFC cycle is shown in the inset of Fig. 10. The two lines split approximately at 30 K and are a further estimate of the quasistatic glass-transition temperature. These experiments have been conducted in different fields and the resulting E, T phase diagram is shown in Fig. 10. All data points up to fields of 1 kV/mm are close to 30 K and show no significant field dependence. In zero random fields the AT line should depend with the power of 1.5 on the external field (dashed line). The exponent was predicted to decrease below unity (Blinc *et al.*, 1989) with increasing random fields (solid line in Fig. 10). While this scenario is not unrealistic we have to state clearly that from the present experiments no analysis concerning the strength of the random field can be made as we have one free parameter which

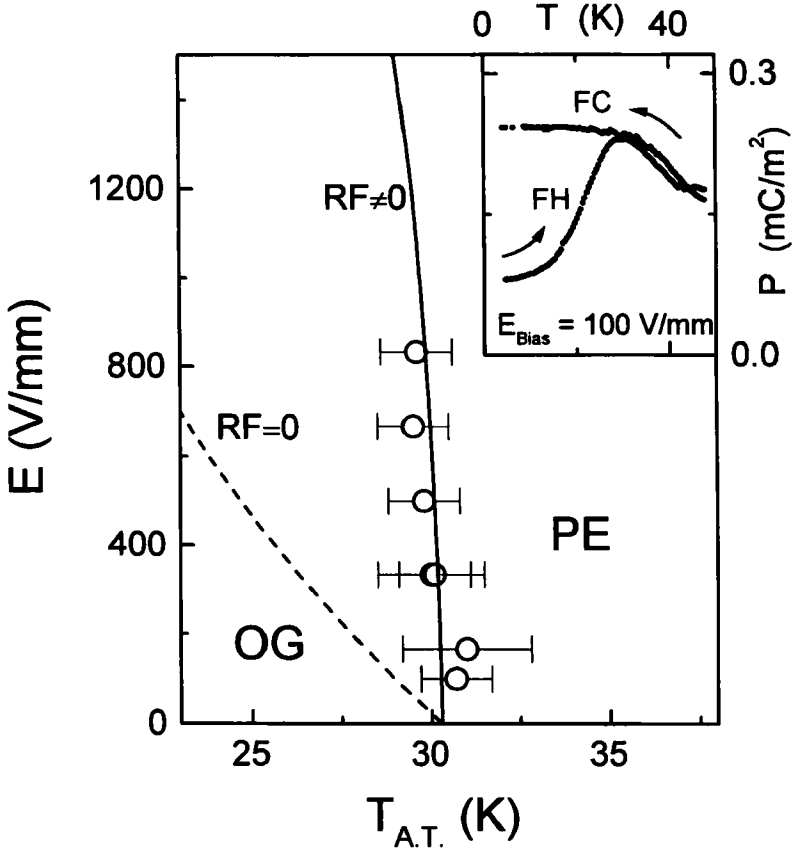

FIGURE 10 Almeida–Thouless line of stability determined by evaluating the splitting of the field cooled and zero-field cooled polarization. A typical measurement is shown in the inset for a field of 100 V/mm and a temperature ramping of 1 K/min. The solid lines are calculations due to a MF-model (Blinc *et al.*, 1989) with ($RF \neq 0$) and without ($RF = 0$) random fields.

can only be determined from the saturation of the AT line towards low temperatures. Hence, the experiments have to be performed at considerably larger external fields which is almost impossible using standard preparation techniques. In the most favorable cases we were able to achieve external electric fields of 1.5 kV/mm.

As we have pointed out earlier the linear susceptibility is not the best suited quantity to study the freezing transition in orientational glasses. One should rather investigate the spin-glass (dipole-glass)

susceptibility (Eq. (4)) which plays the same role in spin-glasses (dipolar glasses) as the uniform susceptibility in ferromagnetic (FE) materials. For small external fields the spin-glass susceptibility is related to the nonlinear susceptibility which exhibits a critical singularity at the glass-transition temperature (Eq. (6)). In D-$BP_{40}BPI_{60}$ we tried to determine the nonlinear susceptibility using two different experimental routes. We measured $P(E)$ hysteresis loops and analyzed the data in terms of an expansion of the polarization in powers of the external field (Eq. (1)). A representative result of these experiments is documented in Fig. 11. Here the real and the imaginary part of the first, second and third-order susceptibilities are shown as a function of temperature. These experiments were performed at a frequency of 33 Hz and a peak to peak voltage of approximately 2 kV/mm. The linear susceptibility reveals a broad smeared out cusp at the freezing temperature. The freezing is also signaled via a significant loss peak. In third order the typical shapes of the real and imaginary part of the susceptibility are observed. Astonishingly we also detected significant contributions in the second-order susceptibility. On the basis of naive field-reversal arguments and in the absence of symmetry breaking local fields no second-order contributions should be detected. However, it has been shown by Vollmayr *et al.* (1994) that in a three-state Potts-glass χ_2 does not vanish. From Fig. 11 it becomes clear that also the higher-order susceptibilities are dominated by dispersion effects. Hence, to use a concept of a diverging third order susceptibility, only this fraction of high-temperature data can be used which is free of dispersion effects. To do so, we determined in a second experiment the third-order susceptibility using an ac technique at a measuring frequency of 90 Hz in a bias field of 1 kV/mm. The result of these measurements is shown in Fig. 12. For comparison we also plotted the real and imaginary part of the linear susceptibility. It is important to note that the third-order susceptibility strongly increases where the linear susceptibility is almost temperature independent. Loss phenomena become visible below 50 K and this data have been excluded in the analysis of the higher-order susceptibility. We analyzed the temperature dependence of χ_{nl} using the scaling ansatz $\chi_{nl} = \chi_1^4/(T - T_f)$. The solid line in Fig. 12 represent the result of the best fit yielding a value of the glass-transition temperature $T_f = 28$ K.

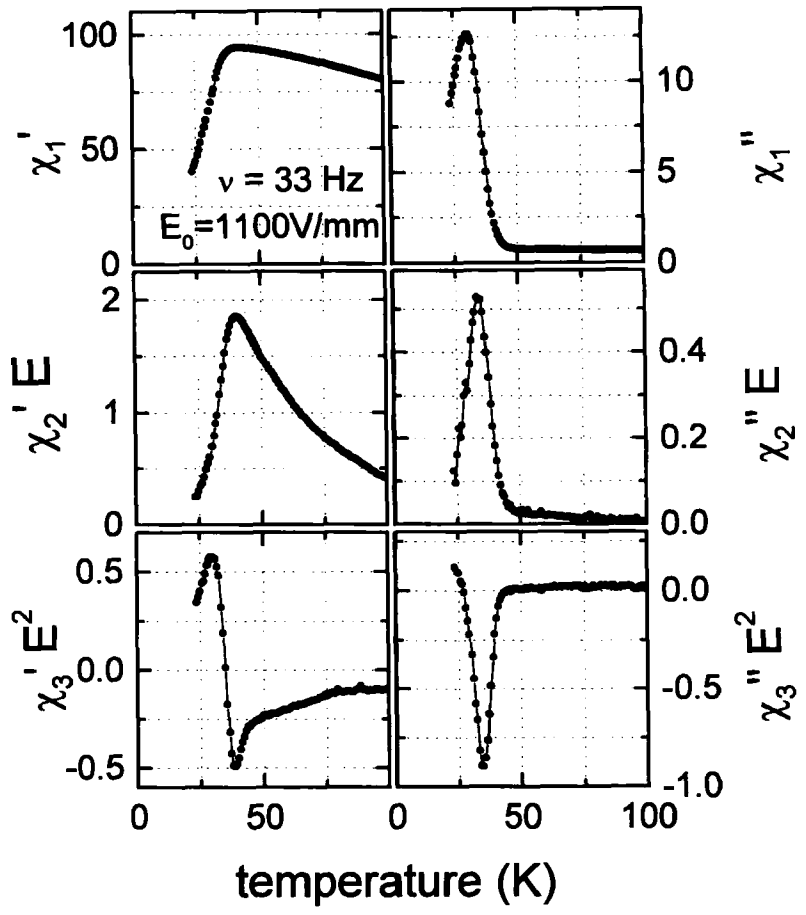

FIGURE 11 Real and imaginary parts of the first three orders of susceptibility vs temperature in D-$BP_{40}BPI_{60}$. The data were evaluated via Fourier-analysis of the polarization signal, driven by a harmonic alternating field with amplitude $E_0 = 1100\,\mathrm{V/mm}$ and frequency $\nu = 113\,\mathrm{mHz}$.

It also seems important to determine the frequency dependence of the mean relaxation times from the nonlinear susceptibility. One could speculate that the higher-order susceptibility follows a power or Vogel–Fulcher law and hence, reveals a stronger temperature dependence than the linear component. We were able to follow the third-order susceptibility in a frequency range from 10 mHz to 100 Hz. A representative result is shown in Fig. 13. Here the real and the

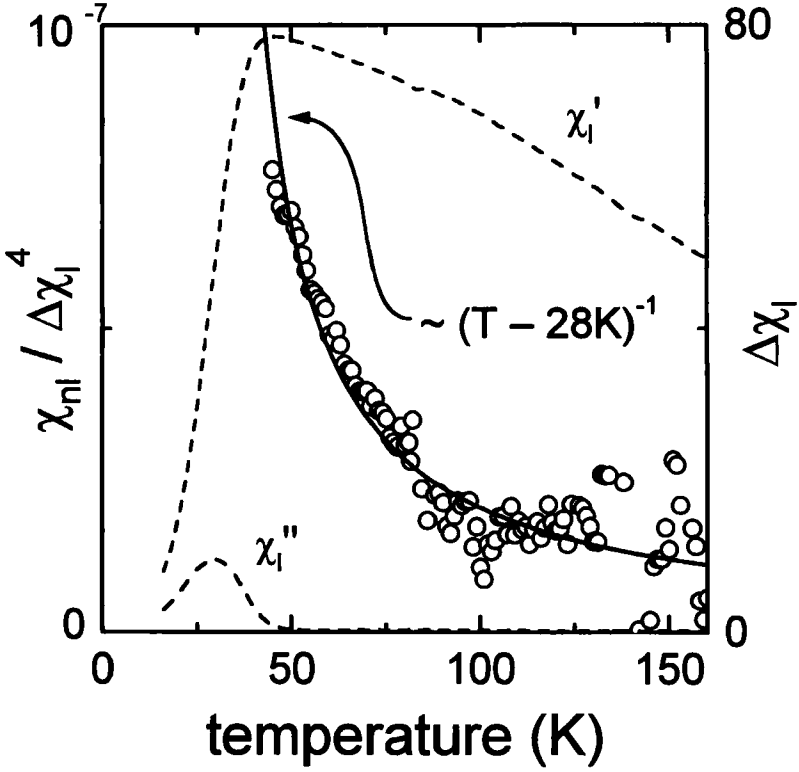

FIGURE 12 Temperature dependence of the nonlinear (third-order) susceptibility in D-$BP_{40}BPI_{60}$ presented as $\chi_{nl}/\Delta\chi_l^4$. The data were measured using a bias field of $E_{Bias} = 1000$ V/mm and a small alternating field. The solid line is calculated as $\chi_{nl}/\Delta\chi_l^4 \propto (T - T_f)^{\gamma}$ with $\gamma = 1$ and $T_f = 28$ K. The dashed lines show real and imaginary parts of the orientational component of the linear susceptibility $\Delta\chi_l^*$.

imaginary part of the third-order susceptibility are plotted versus the measuring frequency for different temperatures between 25 and 42 K. The data indicate an increasing width with decreasing temperatures. To determine the slowing down of the dipolar relaxations viewed via the third-order susceptibilities the characteristic temperatures have been plotted as a function of the inverse temperature. In Fig. 14 the temperatures of the roots and of the maxima of the real part and the minima of the imaginary part of the third-order susceptibility are compared with the peak maxima of the dielectric loss as observed in the linear measurements. Astonishingly all these quantities follow

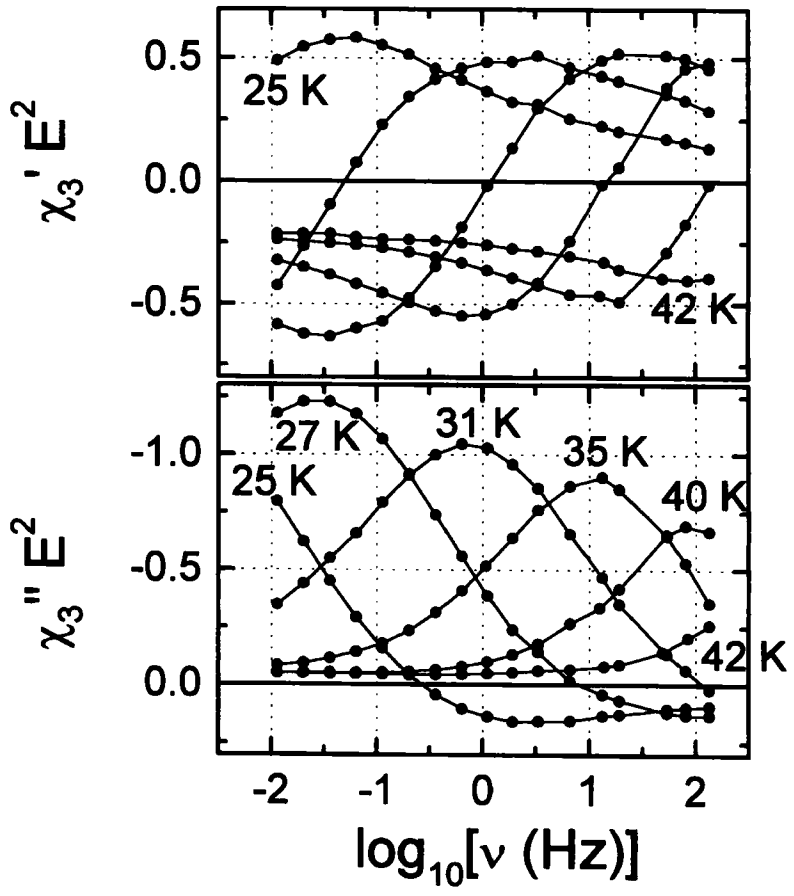

FIGURE 13 Frequency dependence of the complex third-order susceptibility in D-$BP_{40}BPI_{60}$ for several temperatures. The amplitude of the driving signal was 1100 V/mm.

Arrhenius laws with very similar energy barriers. The minima of χ_1'' and χ_3' coincide as predicted from Table I. Hence no criticality can be observed in the temperature dependence of the relaxation rates observed in the higher-order susceptibilities either.

Assuming a constant distribution of activation energies (a linear temperature dependence of the symmetric width parameter) and a purely activated behavior of the relaxation rates the data can be

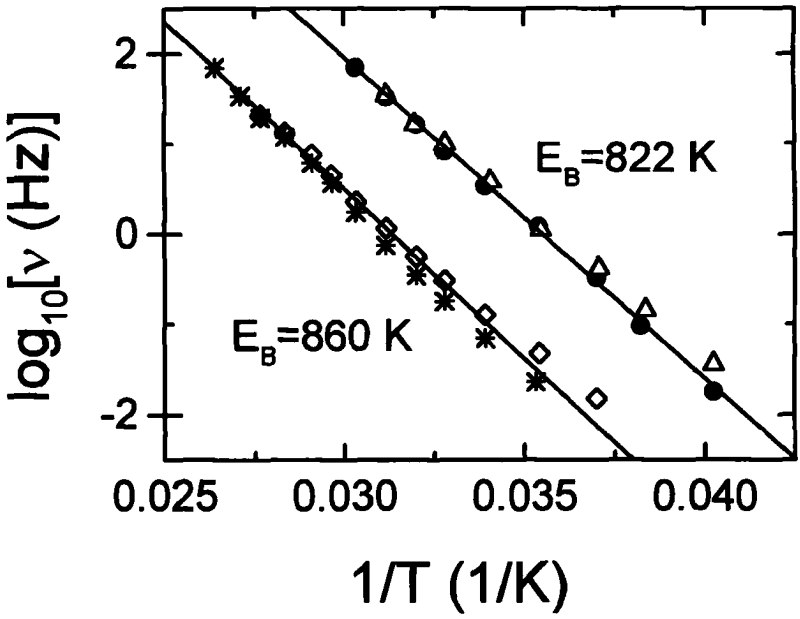

FIGURE 14 Arrhenius-representation due to the significant points of third-order susceptibility-spectra: Maxima in χ_1'' (•) and χ_3' (△), minima in χ_3'' (∗) and roots in χ_3' (◇). The lines are calculations due to thermally activated behavior. The difference in the resulting effective energy barrier is reflecting the broadening of the spectra as a consequence of the broad distribution of energy barriers.

scaled to one master curve (Fig. 15). All data collapse to the curve measured at 31 K which has been chosen arbitrarily as master function. From the superposition of different temperature scans a much wider frequency range can be investigated. All data point toward a rather symmetric distribution of relaxation rates and a rather normal behavior of the frequency dependence of the nonlinear susceptibility as would be observed in a noninteracting dipole system with random fields. That the situation is not so clear is shown in the last figure of this communication. Figure 16 shows Cole–Cole-like representations of the linear and of the third-order susceptibility. In both plots different temperatures have been used to gain representative plots. The linear susceptibilities clearly reveal asymmetric semi-circles characteristic of Havriliak–Negami distributions of relaxation rates. The

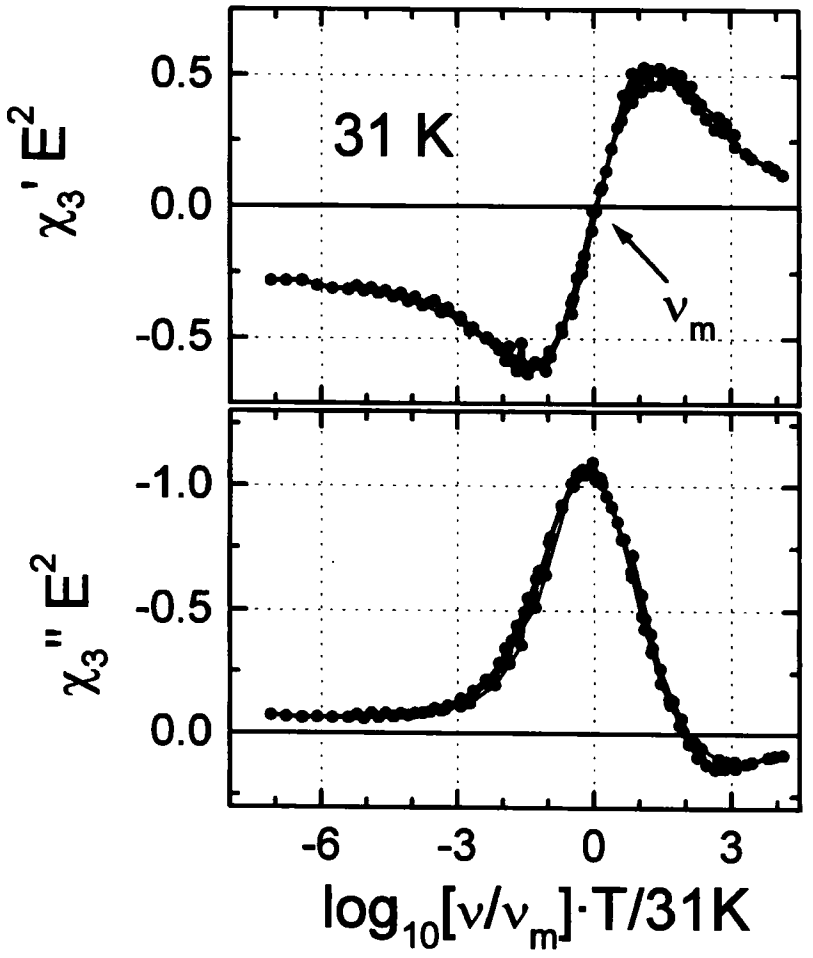

FIGURE 15 "Master"-plot of the data shown in Fig. 14. The curves were scaled on the 31 K spectra due to the discovered reciprocal temperature dependence of the line width of the linear data.

third-order susceptibilities extend into the second and third segment, a clear indication of the third order. However, from a comparison with the model calculations of Fig. 4 it becomes clear that these data cannot be fitted assuming a phenomenological Cole–Cole or Havriliak–Negami distribution of mean relaxation rates and this is again a rather unexpected result.

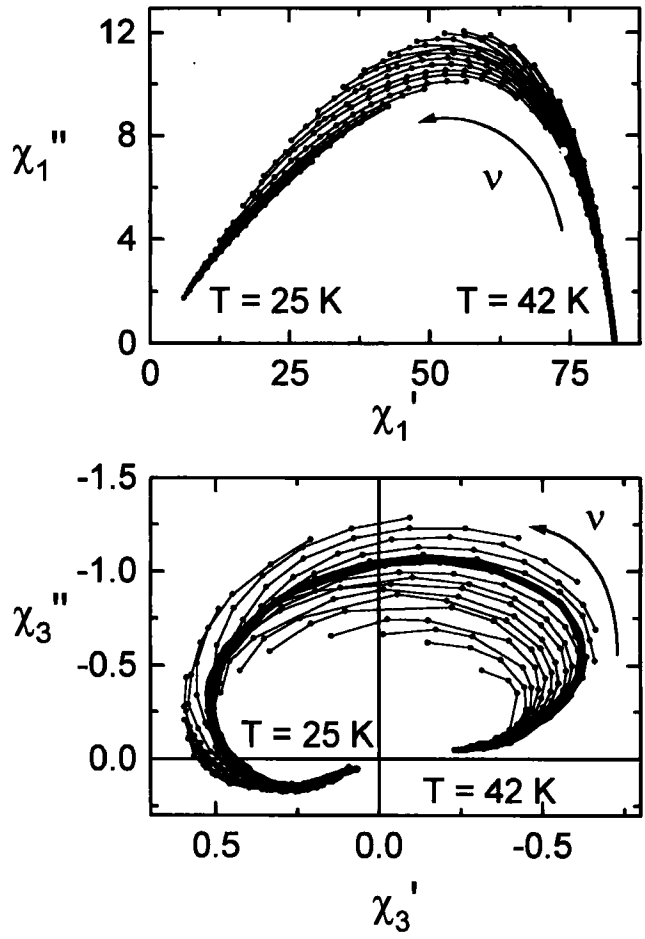

FIGURE 16 Cole–Cole representation of the first and the third susceptibility in D-$BP_{40}BPI_{60}$. The thin lines connect measurements at the same temperature in the frequency range $113\,\text{mHz} < \nu < 131\,\text{Hz}$ for temperatures between 25 and 42 K. The stronger line represents the master-curve shown in Fig. 14.

4 CONCLUSIONS

In this communication we reported field-dependent dipolar susceptibilities in the pure compounds and in the solid solutions of deuterated betaine phosphite and betainephosphate. In the pure compounds we

demonstrated that the nonlinear susceptibilities are ideally suited to detect and study polar phase transitions. In the mixed compounds the relaxation dynamics at the glass transition was studied in detail. Here again we focused on the analysis of the temperature and frequency dependencies of the higher order susceptibilities. We have shown that the second-order susceptibility is nonzero which has been predicted by Vollmayr *et al.* (1994) for three-state Potts models. The temperature dependence of the nonlinear glass susceptibility provides some experimental evidence for a static glass transition temperature close to 30 K. A similar temperature has been determined from FC and ZFC cycles in finite fields and corresponds to the AT line separating the ergodic and the glassy regime. No critical behavior was found in the temperature dependence of the characteristic relaxation rates as determined from the third-order susceptibility. The mean relaxation rates follow a similar Arrhenius behavior as determined from the temperature dependence of the mean relaxation rate from the linear susceptibility component. The third-order susceptibility can be scaled to a unique master curve. However, the Cole–Cole representations of the higher-order susceptibility clearly deviate from model calculations a fact that is not understood at the moment.

Acknowledgements

This research was supported in part by the Sonderforschungsbereich 262 (Mainz). We are indebted to A. Maiazza for growing the high-quality samples.

References

Albers, J., A. Klöpperpieper, H.J. Rother and K.H. Ehses (1982). Anti-ferroelectricity in betaine phosphate. *Phys. Stat. Sol.* (*a*) **74**, 553.

Albers, J. (1988). Betaine compounds – a new family with ferroelectric and incommensurate phases. *Ferroelectrics* **78**, 3.

Alexiewicz, W. (1989). Dispersion and dynamics of third-order electric polarisation in liquids within Smochulinsky–Debye theory. *Physica A* **155**, 84.

Binder, K. and A.P. Young (1986). Spin glasses: experimental facts, theoretical concepts, and open questions. *Rev. Mod. Phys.* **58**, 801; *or* Binder, K. and J.D. Reger (1992). Theory of orientational glasses. Models, concepts, simulations. *Adv. Phys.* **41**, 547.

Blinc, R., J. Dolinsek, B. Tadic, B. Zalar, R. Kind and O. Liechti (1989). Local-polarization distribution in deuteron glasses. *Phys. Rev. Lett.* **63**, 2248.

Brückner, H.J., H.-G. Unruh, G. Fischer and L. Genzel (1988). Dynamical studies of highly deuterated betaine phosphate near the antiferroelectric phase transition. *Z. Phys. B* **71**, 225.

Chalupa, J. (1977). The susceptibilities of spin glasses. *Sol. State Com.* **22**, 315.

Courtens, E. (1987). Mixed crystals of the KH_2PO_4 family. *Ferroelectrics* **72**, 229.

de Almeida, J.R.L. and D.J. Thouless (1978). Stability of the Sherrington–Kirkpatrick solution of a spin glass model. *J. Phys. A* **11**, 983.

Déjardin, J.-L., G. Debias and A. Ouadjon (1993). On the nonlinear behaviour of dielectric relaxation in alternating fields. II. Analytic expressions of the nonlinear susceptibilities. *J. Chem. Phys.* **98**, 8149.

Dixon, P.K. and L. Wu (1989). Broadband digital lock-in amplifier techniques. *Rev. Sci. Instrum.* **60**, 3329.

Fehst, I., M. Paasch, S.L. Hutton, M. Braune, R. Böhmer, A. Loidl, M. Dörffel, Th. Narz, S. Haussühl and G.J. McIntyre (1993). Paraelectric and ferroelectric phases of betaine phosphite: structural, thermodynamic, and dielectric properties. *Phys. Stat. Sol. (b)* **181**, 71.

Hemberger, J. (1997). Dielektrische Spektroskopie am Orientierungsglasübergang: Lineares und nichtlineares Verhalten in Betain-Mischkristallen. Dissertation, TH Darmstadt.

Hemberger, J., H. Ries, A. Loidl and R. Böhmer (1996). Static freezing transition at a finite temperature in a quasi-one-dimensional deuteron glass. *Phys. Rev. Lett.* **76**, 2330.

Höchli, U.T. (1987). Electric dipole glasses. *Cryst. Latt. Def. and Amorph. Mat.* **14**, 275.

Höchli, U.T., K. Knorr and A. Loidl (1990). Orientational glasses. *Adv. Phys.* **39**, 405.

Kutnjak, Z., C. Filipič, A. Levstik and R. Pirc (1993). Glassy dynamics of $Rb_{0.40}(ND_4)_{0.60}D_2PO_4$. *Phys. Rev. Lett.* **70**, 4015.

Levstik, A., C. Filipič, Z. Kutnjak, I. Levstik, R. Pirc, B. Tadić and R. Blinc (1991). Field-cooled and zero-field-cooled dielectric susceptibility in deuteron glasses. *Phys. Rev. Lett.* **66**, 2368.

Loidl, A. and R. Böhmer (1994). Glass transitions and relaxation phenomena in orientational glasses and supercooled plastic crystals, Chapt. 24 from *Disorder Effects on Relaxational Processes*, R. Richert and A. Blumen (Eds.), Springer, Berlin.

Loidl, A., J. Hemberger, M. Winterlich, H. Ries and R. Böhmer (1996). Linear and nonlinear dielectric spectroscopy in dipolar glasses. *Ferroelectrics* **176**, 43.

Maeda, M., T. Atake, Y. Saito and H. Terauchi (1989). Low-temperature specific heats of betaine phosphate and successive phase transition at 82.7 and 87.1 K. *J. Phys. Soc. Japan* **58**, 1135.

Nakada, O. (1960). Theory of non-linear responses. *J. Phys. Soc. Japan* **15**, 2280.

Orihara, H., S. Hashimoto and Y. Ishibashi (1993). A theory of $D-E$ hysteresis loop based on the Avrami model. *J. Phys. Soc. Japan* **63**, 1031.

Pirc, R., B. Tadić and R. Blinc (1994). Nonlinear susceptibility of orientational glasses. *Physica B* **193**, 109.

Sawyer, C.B. and C.H. Tower (1929). Rochelle salt as a dielectric. *Phys. Rev.* **35**, 269.

Schaack, G. (1990). Experimental results on phase transitions in betaine compounds. *Ferroelectrics* **104**, 147.

Suzuki, M. (1977). Phenomenological theory of spinglasses and some rigorous results. *Prog. Theor. Phys.* **58**, 1151.

Vollmayr, K., G. Schneider, J.D. Reger and K.J. Binder (1994). Static magnetic response of the three-state Potts glass. *Non-Cryst. Solids* **172–174**, 488.